REMOTE SENSING STUDIES OF HANSTEEN ALPHA. B. R. Hawke[1], T. A. Giguere[1,2], S. J. Lawrence[3], T. D. Glotch[4], B. T. Greenhagen[5], B. L. Jolliff[6], P. G. Lucey[1], J. D. Stopar[3], C. A. Peterson,[1] D. A. Paige[7], M. S. Robinson[3], and the LROC Science Team, [1]Hawaii Institute of Geophysics and Planetology, University of Hawaii, Honolulu, HI 96822 (hawke@higp.hawaii.edu), [2]Intergraph Corporation, Box 75330, Kapolei, HI 96707, [3]School of Earth and Space Exploration, Arizona State University, Tempe, AZ 85281, [4]Department of Geoscience, Stony Brook University, Stony Brook, NY, [5]Jet Propulsion Laboratory, 4800 Oak Grove Drive, Pasadena, CA 91109-8099, [6]Washington University, One Brookings Drive, St. Louis, MO 63130, [7]Department of Earth and Space Sciences, University of California, Los Angeles, Los Angeles, CA.

Introduction: Hansteen α is an arrowhead-shaped highlands feature located on the southern margin of Oceanus Procellarum just north of the crater Billy (Figures 1 and 3). The feature is a rough-textured triangular mound that is ~25 km on a side and exhibits a relatively high albedo. Hansteen α is a member of a class of lunar spectral anomalies known as red spots which are characterized by a relatively high albedo and a strong absorption in the UV [1,2]. Some early workers presented evidence that at least some red spots were produced by nonmare or highlands volcanism and suggested a connection with KREEP basalts or even more evolved highlands composition (e.g., dacite, rhyolite) [1,2,3]. Recent research using Clementine, Lunar Prospector (LP), and Lunar Reconnaissance Orbiter (LRO) data have provided strong evidence that some red spots are dominated by Th- and silica-rich, highly evolved highlands lithologies [4,5,6,7,8,16,17]. The purpose of this study is to use new images from the Lunar Reconnaissance Orbiter Cameras [9] and LRO Diviner Lunar Radiometer Experiment data [7,8] as well as Clementine UVVIS images to investigate the geology and composition of Hansteen α.

Morphology and Geology: McCauley [10] described Hansteen α as being made up of steep-sided, bulbous, very bright dome material that exhibits a hackly surface. He also described several small, linear, smooth-walled depressions at the crests of gentle individual highs and interpreted these depressions as probable volcanic vents. Wood and Head [1] noted that the dome appeared distinctive in its surface texture, color, and albedo from nearby highlands and is embayed by adjacent mare units. Wagner *et al*. [11] stated that Hansteen α had a flat summit region reminiscent of a mesa and noted that the summit surface as well as the flanks appear much more rugged than the Gruithuisen domes. Wagner *et al.* determined a cratering model age of 3.67 Ga for two areas in the summit region.

LROC Wide Angle Camera (WAC) and Narrow Angle Camera (NAC) images were used to investigate Hansteen α, and to produce DEMs for the region [12]. The outer margin of Hansteen α is marked by a steep slope rising sharply from the surrounding mare surface (Figure 1).

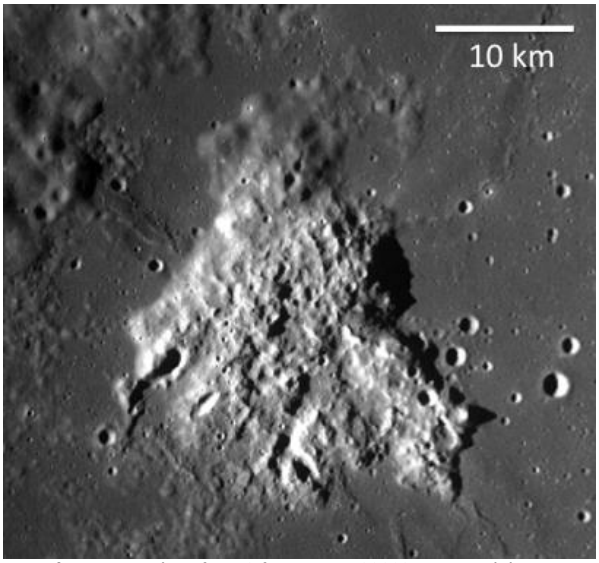

Figure 1. Portion of WAC frame M117826631ME. North is up.

The NE margin of the Arrowhead rises abruptly to a height of ~740 m above the mare surface and has an average slope of 18°. The surface of the summit gently slopes up to the highest point (1036 m) which is located just SW of the center of Hansteen α. The summit surface is rough at a variety of scales. Numerous depressions and ridges can be seen in Figure 1. High-resolution (0.5 meters/pixel) views of the surface of Hansteen α have been provided by LROC NAC frames [17]. Portions of NAC frames covering the central portion of Hansteen α are shown in Figure 2. Numerous depressions can be seen. Many are circular while others are more irregular in shape. Black arrows indicate old, degraded impact craters. White arrows point out more irregular depressions of endogenic origin. Some of these have been interpreted as volcanic vents by McCauley [10]. Alternately, many of these depressions may be collapse features related to the emplacement of silicic flows.

Composition: Clementine UVVIS images were used to produce FeO, TiO_2, and optical maturity maps of the Hansteen α region utilizing the algorithms of Lucey *et al*. [13,14]. Mare units in this region exhibit FeO abundances >16wt%, and TiO_2 values range betteween 4wt% and 8wt%. In sharp contrast, much lower FeO and TiO_2 values are exhibited by Hansteen α.

FeO values range from 5wt% to 9wt% with slightly higher values occurring near the highland/mare contact. Most of Hansteen α exhibits <1wt% TiO_2. The central, core portion of the feature has an average FeO value of 6.9wt% and an average TiO_2 value of 0.5wt%. Since this central region has suffered the least amount of contamination by surrounding mare units, its composition may most closely approximate that of the underlying lithology. The Imbrian-aged craters Billy and Hansteen emplaced relatively FeO- and TiO_2-rich ejecta. Hansteen α exhibits much lower FeO and TiO_2 values. If the dome was present prior to the formation of Billy and Hansteen craters, it should have been covered with FeO- and TiO_2-rich ejecta since it is within one crater diameter of the rim crest of each crater. Since it is not, Hansteen α was emplaced on top of the FeO-rich ejecta deposits. Nonmare volcanism is the only viable process for the formation of Hansteen α.

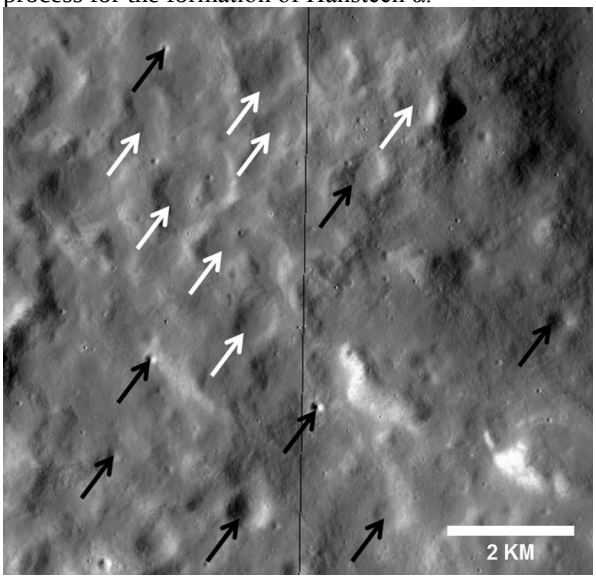

Figure 2. Portions of NAC frames M181501799L&R. North is up.

Lawrence *et al*. [5] used forward modeling to show that the Th abundance at Hansteen α is not 6 ppm, as indicated by the LP-GRS Th map, but is more likely closer to 25 ppm. A more recent forward modeling study by Hagerty *et al*. [6] reported a Th abundance of 20 ppm for Hansteen α. High Th values in the 20 to 25 ppm range are consistent with Th abundances measured in evolved lunar lithologies such as granites and felsites.

The Diviner Lunar Radiometer Experiment on the LRO is a multispectral radiometer that is well suited to detecting the mineral indicators of silicic volcanism [7]. Diviner has three narrow spectral bandpass filters centered at 7.8, 8.25, and 8.55 μm that were specifically designed to characterize the position of the Christiansen Feature [8,15], which is directly sensitive to silicate mineralogy and the bulk SiO_2 content of a lithology [7]. Glotch *et al*. [7] used Diviner three-point spectra and two spectral parameters (C and I) that describe the spectra to investigate variations in silicate mineralogy and to search for the key indicators of silicic volcanism (quartz, silica-rich glass, and alkali feldspars). They determined that portions of four red spots (Hansteen α, Gruithuisen domes, Lassel massif, and Aristarchus south rim and ejecta) had spectral parameter or index values best explained by Si-rich glass, quartz, and/or alkali feldspars.

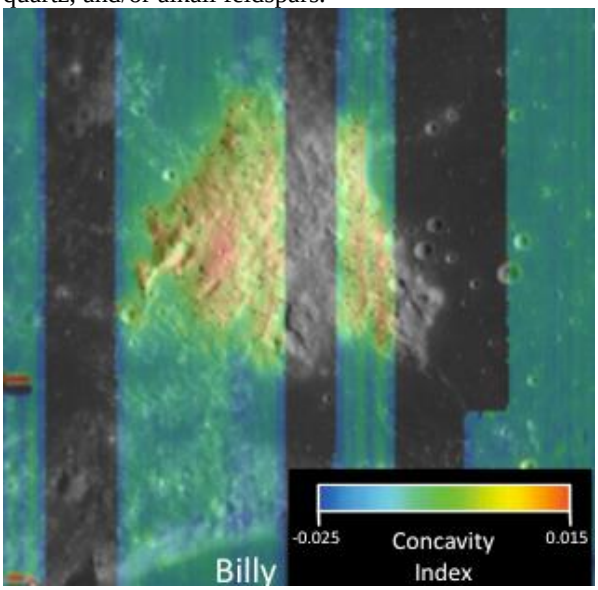

Figure 3. Diviner concavity map overlaid on WAC frame. North is up.

The C parameter or concavity index provides an estimate of the abundance of silicic materials. Figure 3 shows the most recent concavity index map of the Hansteen α region overlaid on a WAC image (M11782663ME). High values of the index (red) indicate increasingly silicic compositions. Lower concavity index values are green and blue. High values are more abundant near the center of Hansteen α and in the high terrain SW of the center. The lower values on the margins of the feature may be the result of contamination by mare debris transported to the lower slopes of the dome by impacts in the surrounding mare.

References: [1] Wood, C. and Head, J.W. (1975) *Conf. on Origins of Mare Basalts*, 189. [2] Head, J. and McCord, T. (1978) *Science, 199*, 1433. [3] Malin, M. (1974) *EPSL, 21*, 331. [4] Hawke, B. *et al.* (2003) *JGR, 108(E7)*, 5069. [5] Lawrence, D. *et al.* (2005) *GRL, 32*, L0721. [6] Hagerty, J. *et al.* (2006) *JGR, 111*, E06002. [7] Glotch, T. *et al.* (2010) *Science, 329*, 1510. [8] Greenhagen, B. *et al.* (2010) *Science, 329*, 1507. [9] Robinson, M. *et al.* (2010) *Space Sci. Rev., 150*, 81. [10] McCauley, J. (1973) *U.S.G.S. Map I-740*. [11] Wagner, R. *et al.* (2010) *JGR, 115*, E06015. [12] Scholten, F. *et al.* (2012) *JGR, 117*, 12 pp. [13] Lucey, P. *et al.* (2000) *JGR, 105(E8)*, 20,297. [14] Lucey, P. *et al.* (2000) *JGR, 105(E8)*, 20,377. [15] Paige, D. *et al.* (2010) *Space Sci. Rev., 150*, 125. [16] Glotch, T. *et al.* (2011) *GRL, 38*, L21204. [17] Hawke, B. *et al.* (2011) *LPS 42nd*, Abs. 1652.